







Single Sideband Signals for Phase Noise Mitigation in Wireless THz-Over-Fibre Systems

Luis Gonzalez-Guerrero , Haymen Shams , *Member, IEEE*, Irshaad Fatadin, *Senior Member, IEEE*,
Martyn J. Fice , *Member, IEEE*, Mira Naftaly , Alwyn J. Seeds , *Fellow, IEEE*,
and Cyril C. Renaud , *Senior Member, IEEE*

Abstract—In future photonic-based THz backhaul links, integrating the optical local oscillator (LO) in a remote antenna unit can be beneficial in terms of optical bandwidth efficiency and higher compatibility with passive optical networks. In such a scenario, two approaches can be used to reduce the high phase noise associated with free-running lasers: 1) baseband (BB) signals & carrier recovery, and 2) single sideband (SSB) signals & envelope detection. In this paper, we compare the performance of the two approaches for various optical LO linewidths using 5 GbD 16-QAM signals. We find that, for a total linewidth wider than 0.55 MHz, the SSB approach yields better results. The superior performance, however, comes at the expense of reducing the net information spectral density (ISD) of the SSB signal by 39% compared to that of the BB signal. However, using signal–signal beat interference-mitigation algorithms, an ISD only 15% lower than the BB signal ISD was sufficient to meet the FEC requirement. Given these results, we believe that the envelope detection of SSB signals is a promising solution to mitigate the phase noise problem of THz links based on free-running lasers, without excessively compromising the spectral efficiency of the system.

Index Terms—Broadband communication, digital signal processing, envelope detectors, microwave photonics, millimeter wave communication, optical mixing, photonic integrated circuits, semiconductor lasers.

I. INTRODUCTION

PHOTONICS-BASED THz communications, while enabling a seamless integration with optical fibre networks [1], have the disadvantage of suffering from phase noise penalties [2]. This, which results from the broad linewidths associated

Manuscript received February 13, 2018; revised July 19, 2018; accepted July 20, 2018. Date of publication August 9, 2018; date of current version August 30, 2018. This work was supported in part by the Engineering and Physical Sciences Research Council through the COTS (EP/J017671/1) and COALESCE (EP/P003990/1) grants, in part by the European Commission through the European project iPHOS under Grant 257539, in part by the European Union’s Horizon 2020 research and innovation programme under Grant 761579 (TER-APOD), in part by the project EMPIR 14IND13 PhotInd at NPL, in part by the EMPIR programme co-financed by the Participating States, and in part by the European Union’s Horizon 2020 research and innovation programme. (Corresponding author: Luis Gonzalez-Guerrero.)

L. Gonzalez-Guerrero, H. Shams, M. J. Fice, A. J. Seeds, and C. C. Renaud are with the Department of Electronic and Electrical Engineering, University College London, London WC1E 7JE, U.K. (e-mail: uceelgo@ucl.ac.uk; h.shams@ucl.ac.uk; m.fice@ucl.ac.uk; a.seeds@ucl.ac.uk; c.renaud@ucl.ac.uk).

I. Fatadin and M. Naftaly are with the National Physical Laboratory, Teddington TW11 0LW, U.K. (e-mail: irshaad.fatadin@npl.co.uk; mira.naftaly@npl.co.uk).

Color versions of one or more of the figures in this paper are available online at <http://ieeexplore.ieee.org>.

Digital Object Identifier 10.1109/JLT.2018.2864145

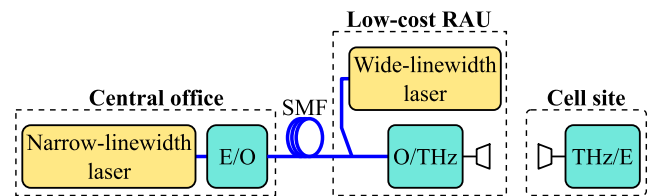


Fig. 1. THz backhaul link based on photonic technologies. E/O: electrical-to-optical converter, O/THz: optical-to-THz converter, THz/E: THz-to-electrical converter.

with commercial free-running lasers, is a major impediment for their commercial implementation [3]. Solutions based on filtering two optical modes of an optical frequency comb generator (OFCG) have been proposed to mitigate this problem [4]. However, this approach requires the use of narrow and tuneable optical filters, external modulators and radio-frequency (RF) local oscillators (LOs), which would increase significantly the complexity of the transmitter [5]. Free-running lasers, on the other hand, remain attractive to internet providers because of their simplicity, cost and tuneability capabilities [6]. Furthermore, the use of these lasers allows the optical LO to be placed at the remote antenna unit (RAU). This architecture, which has already been investigated for mm-wave links [7], can be beneficial in terms of optical bandwidth efficiency and integration with passive optical networks (PONs). In such a case, the cost of the LO laser must be kept low to maintain a competitive price per RAU. This requirement calls for foundry-fabricated semiconductor lasers (linewidths > 1 MHz) to be used in the antenna unit. In Fig. 1 we show the implementation scenario that we envisage within this paper. Note that, in the central office (CO), where the total cost is shared between all the users supported by the network, volume-production semiconductor lasers with linewidths in the range of a few hundreds of kHz are economically acceptable [8].

Given the scenario depicted in Fig. 1, alternative ways for phase noise mitigation (other than OFCG filtering) must be found. A potential solution to this problem, is the use of advanced digital signal processing (DSP) techniques for carrier recovery at the receiver. These algorithms normally comprise two steps: (a) compensation of the frequency offset between signal and LO and (b) cancellation of the phase noise distortions (arising mainly from the lasers’ linewidths). Before eliminating these impairments, the phase distortion (intentionally

introduced by the data, needs to be removed. This can be done with the Viterbi-Viterbi (VV) algorithm, which raises the incoming samples to the M^{th} power (where M is the modulation order of the modulation format). Although the VV algorithm was originally intended for phase shift keying (PSK) signals, it can be adapted to square QAM constellations [9]. After removing the data, the frequency offset can be estimated with a fast Fourier transform (FFT) [10] and the phase noise with an averaging filter to remove the phase distortions caused by additive white Gaussian noise (AWGN) [9].

One of the drawbacks of the square QAM-adapted VV algorithm presented in [9] is that not all the received samples are used to calculate the symbol deviations introduced by phase noise. To solve this, more complex adaptations of the VV algorithm [11] or completely different approaches not relying on the M^{th} power operation [12] have been proposed. Although these algorithms exhibit better performance, their implementation complexity is also higher [13]. In this comparison, we choose the algorithm in [9] due to its simplicity and the fact that the VV algorithm is a well-established technique in the communications community [14].

Another approach that has been extensively used for phase noise mitigation in the RF [15] and optical domains [16] is the use of single sideband (SSB) signals together with envelope detection. This technique has also been proposed to enable the use of free-running lasers in high-frequency radio-over-fibre (RoF) systems [7]. The analytical analysis proving its phase robustness has been shown extensively in literature (see for instance [17]). Experimentally, however, RoF demonstrations have been limited to systems using fixed-linewidth optical sources, where verifying its insensitivity to phase noise was not possible [18]. In this work, we assess the performance of this scheme in a RoF link with the configuration shown in Fig. 1 and varying linewidths of the RAU laser. The linewidth tuning is achieved by means of digital modulation, which, unlike other linewidth tuning mechanisms such as power tuning, does not compromise other characteristics of the laser [19].

Apart from allowing the use of low cost lasers, this approach also relaxes the complexity of the carrier recovery DSP and does not require a THz LO at the receiver, greatly simplifying the system architecture. On the other hand, one of the problems with SSB envelope-detected signals is the signal-signal beat interference (SSBI). This impairment, which results from the overlap of the direct detection (DD) terms with the signal of interest, results in a reduced system sensitivity. Because of this, at narrower laser linewidths, this technique is expected to yield worse results than the approach of using baseband (BB) signals together with carrier recovery. However, since the performance of the VV algorithm degrades at broad optical linewidths [9], the SSB scheme should become better owing to its phase noise insensitivity. The degradation of the VV algorithm is caused as the averaging filter is shortened to track the faster phase deviations introduced by broader linewidths. The shorter the averaging filter the less effective it becomes against AGWN and, hence, the higher the signal-to-noise ratio (SNR) needs to be to produce a pre-determined bit error rate (BER).

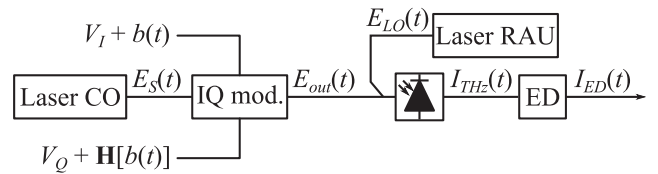


Fig. 2. Schematic depiction of the proposed system for the photonic generation of THz SSB signals.

To determine the linewidth at which the sensitivity of the SSB technique becomes superior, we perform a second linewidth-emulation experiment but this time in a system transmitting BB signals, and then compare the results with those obtained for SSB signals. All the transmissions are performed using 16-QAM signals as this spectrally-efficient modulation format is considered key to achieving the data rates that are expected from the THz range [20]. Before characterizing the phase-noise tolerance of SSB signals, we measure their performance using different guard bands (GBs) between carrier and signal. This is done to determine the highest spectral efficiency allowed by our system (i.e., the lowest GB that could be successfully recovered). The use of these GBs is a common approach to reduce the impact of the SSBI. However, this practice comes at the expense of reducing the spectral efficiency of the SSB signal (i.e., wider GBs reduce the SSBI but also the spectral efficiency).

In the experiment reported here, due to the lack of a THz envelope detector (ED), the envelope detection was implemented in the digital domain after analog-to-digital conversion. Because of this, a THz LO was necessary to down-convert the SSB signals to an intermediate frequency (IF). It should be noted that this configuration was only intended to replicate the performance of a system with an analog ED.

The rest of the paper is organized as follows. In Section II, a brief mathematical analysis of the generation and detection of THz SSB signals is provided. In Section III, the experimental arrangement, including the transmitter and receiver DSP, for the transmission and detection of BB and SSB signals is described. In Section IV, the performance of each scheme for different LO linewidths (and GBs in the case of SSB signals) is presented in terms of BER. In Section V, we analyse and compare the results and estimate the linewidth that is required for the SSB signals to yield a lower penalty at the forward error correction (FEC) limit. Finally, in Section VI, we summarize the main findings of the paper.

II. GENERATION OF SPECTRALLY-EFFICIENT THz SSB SIGNALS THROUGH OPTICAL HETERODYNING

In this section, we obtain an analytical expression for the output of the ED to identify critical parameters when generating THz SSB signals through optical heterodyning. In this scheme, the SSB wireless signal is generated by mixing an optical SSB signal with an unmodulated optical tone in an ultra-fast photodiode (PD), as shown in Fig. 2. To enable the transmission of spectrally-efficient QAM SSB signals, the BB signal is first up-converted to an RF-subcarrier frequency. This signal, together

with its Hilbert transform (in Fig. 2 denoted by $\mathbf{H}[\bullet]$), is then fed to an IQ-modulator, which, assuming a small modulation index, linearly maps it to the optical domain producing an optical SSB signal. After fiber transmission, the optical SSB signal is coupled with an optical LO laser oscillating at an offset frequency corresponding to the THz transmission frequency. At the output of the coupler, an ultra-fast PD is used to mix the two laser modes and generate the SSB THz signal. After wireless transmission, the ED brings the THz signal back to the RF-subcarrier frequency.

The up-converted signal, $b(t)$, and the output of the lasers at the CO, $E_S(t)$, and RAU, $E_{LO}(t)$, can be written as:

$$b(t) = A_{\text{mod}}(t) \cos(\omega_{SC}t + \theta_{\text{mod}}(t)), \quad (1)$$

$$E_S(t) = A_S \exp[j[\omega_S t + \varphi_S(t)]], \quad (2)$$

$$E_{LO}(t) = A_{LO} \exp[j[\omega_{LO}t + \varphi_{LO}(t)]], \quad (3)$$

where $A_{\text{mod}}(t)$ and $\theta_{\text{mod}}(t)$ are the amplitude and phase terms of the data signal, respectively, and ω_{SC} is the angular RF-subcarrier frequency. On the other hand, $A_S(t)$ and $A_{LO}(t)$ are the optical field amplitudes and $\varphi_S(t)$ and $\varphi_{LO}(t)$ are the phase noise terms of the CO and RAU lasers, respectively.

The THz SSB signal generated at the ultra-fast PD is given by the product of the IQ mod. output, $E_{\text{out}}(t)$, and $E_{LO}(t)$ phase-shifted by 90° (due to the 3-dB optical coupler):

$$\begin{aligned} I_{THz}(t) &\propto E_{\text{out}}(t) \cdot (jE_{LO}(t))^* \\ &\propto A_C \exp[j[\omega_{THz}t + \Delta\varphi(t) + \theta_{bias}]] \\ &\quad + A_{\text{mod}}(t) \exp[j[(\omega_{THz} + \omega_{SC})t + \theta_{\text{mod}}(t) + \Delta\varphi(t)]], \end{aligned} \quad (4)$$

where $\omega_{THz} = |\omega_S - \omega_{LO}|$ is the THz frequency, and $\Delta\varphi(t) = \varphi_S(t) - \varphi_{LO}(t) - \pi/2$ represents the phase noise of the THz signal and includes the 90° degree phase shift introduced by the coupler. On the other hand, $\theta_{bias} = \arctan(V_Q/V_I)$ is a phase offset between the carrier (first term in (4)) and the sideband (second term in (4)) caused by the biasing points of the I- and Q-components in the IQ modulator (V_I and V_Q , in Fig. 2, respectively) [21], and $A_C = (V_Q + V_I)^{1/2}$.

Finally, modelling the ED as a square-law device where the output is low pass filtered, the final signal can be expressed as:

$$\begin{aligned} I_{ED}(t) &\propto I_{THz}(t) \cdot I_{THz}^*(t) \\ &\propto A_C^2 + A_{\text{mod}}^2(t) \\ &\quad + 2A_C A_{\text{mod}}(t) \cos(\omega_{SC}t + \theta_{\text{mod}}(t) + \theta_{bias}). \end{aligned} \quad (5)$$

As can be seen from (8), the detected signal includes a DC component (first term), the SSBI component (second term), which spans from DC up to the signal bandwidth (BW), and the desired signal at ω_{SC} (third term), which extends from the GB to $\text{GB} + \text{BW}$. From this, it is easy to see that, to totally cancel the SSBI, the GB must be equal to the BW.

Note that the recovered signal in (5) does not include the combined phase noise contribution of the two lasers $\Delta\varphi(t)$ since it vanishes when the unmodulated tone beats with the sideband

in the ED. On the other hand, it does contain θ_{bias} , which needs to be removed during the demodulation process.

As was previously mentioned, in this experiment, the THz SSB signal is first down-converted before being fed to the digital ED. For this step, a second harmonic mixer (SHM) driven by the output of a $\times 6$ multiplier was used. As such, the phase noise contribution of the THz LO is that of the synthesiser driving the multiplier scaled by a factor of 12. However, since this contribution is also passed both to the tone and sideband of the SSB signal, it vanishes when these components beat in the ED (i.e., in the mathematical analysis this contribution could be included in $\Delta\varphi(t)$ without changing the result).

The carrier-to-sideband power ratio (CSPR), defined as

$$\text{CSPR(dB)} = 10 \log_{10} \left(\frac{A_C^2}{\langle A_{\text{mod}}^2(t) \rangle} \right), \quad (6)$$

is an important parameter in systems using envelope detection. SSB signals with low CSPR suffer from high SSBI, while high CSPR leads to reduced signal-to-noise ratio (SNR). Thus, it is important to ensure the system always operates at the optimum CSPR value. With narrow GBs, the system is limited by SSBI and high values of CSPR are required to compensate it. Wide GBs, on the other hand, can reduce or completely eliminate the SSBI, allowing operation at lower CSPRs to increase the SNR of the received signal [22]. When using the Hilbert transform and an IQ-modulator to generate the SSB signal, the tuning of the CSPR is achieved by adjusting the biasing points of the I- and Q-components. To achieve high CSPRs (i.e., narrow GBs), the biasing points must be set close to the quadrature point. On the other hand, to reduce the CSPR (i.e., wide GBs), the modulator must be biased close to the null point.

It is also important to mention that, in order to achieve a high optical sideband suppression ratio (OSSR), the signals driving the IQ-modulator must be amplitude-, phase- and time-matched (i.e., there is no IQ imbalance). If that is the case, then the maximum OSSR achievable is approximately equal to the extinction ratio (ER) of the optical modulator [23]. For amplitude and phase channel response corrections, a digital pre-equalization technique such as the one presented in [24] can be used. For time-matching, two phase shifters may be placed in each electrical arm of the IQ-modulator.

III. EXPERIMENTAL PROCEDURE

A. Transmitter DSP

The DSP blocks used to generate the BB and SSB signal waveforms are shown in Fig. 3(a) and (b), respectively. In both cases, four 2^{11} de Bruijn bit sequences were mapped into 5 GBd 16-QAM symbols. For BB signal transmission, the I- and Q-components obtained after applying a pair of root raised cosine (RRC) filters with roll-off factors of 0.1 (giving a BW of 5.5 GHz), were directly uploaded to the arbitrary waveform generator (AWG), which operated at a sample rate of 50 Gsample/s. For the generation of SSB signals, the RRC-shaped signal was then digitally up-converted to f_{SC} by feeding it to a digital IQ modulator. After this, a Hilbert transform was applied to the Q-component to remove the lower frequency sideband.

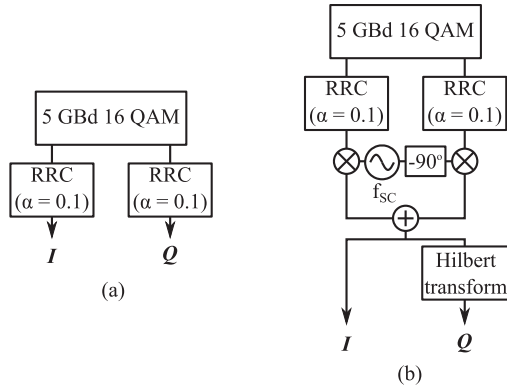


Fig. 3. Transmitter DSP for (a) BB signals and (b) SSB signals. α : Nyquist roll-off factor.

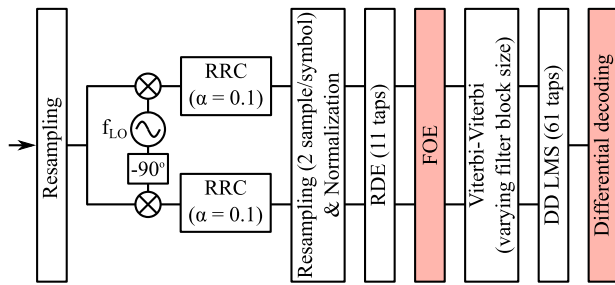


Fig. 4. Blocks of the receiver DSP (red blocks were only used for BB signals). f_{LO} : frequency of the digital demodulator LO (in the case of SSB signals $f_{LO} = f_{SC}$).

B. Receiver DSP

The DSP blocks used to recover both the BB and SSB signals are shown in Fig. 4 (blocks in red were only used for BB signals). In both cases, the digitalized signal was first fed into a digital IQ demodulator for down-conversion. After this, a coherent DSP routine consisting of: matched filtering, resampling & normalization, carrier recovery, and equalization was carried out. The equalizer was initialized using the radius directed algorithm (RDE) and then switched to a decision-directed least mean squares (DD-LMS) mode equalizer. Before switching to the DD-LMS equalizer, the carrier recovery stage was applied to compensate for phase and frequency distortions. In the case of the BB signals, this stage comprised (a) the FFT-based frequency offset estimation (FOE) [10] and (b) the block M^{th} -power algorithm [9]. The sample length of the averaging filter (N) was optimized for each optical LO linewidth. In the case of the SSB signals, only the block M^{th} -power algorithm was used at this stage. Note that this step was only required to compensate for the fixed phase offset introduced by the biasing points of the modulator (θ_{bias} in (5)), and a very high block size ($N = 600$) could be used for all LO linewidths (i.e., no optimization of N was required for each linewidth). After the DD-LMS, differential decoding of the first two bits was carried out in the case of BB signals to avoid cycle slips [25]. Finally, the quality of the received signals was measured in terms of BER and error vector magnitude (EVM).

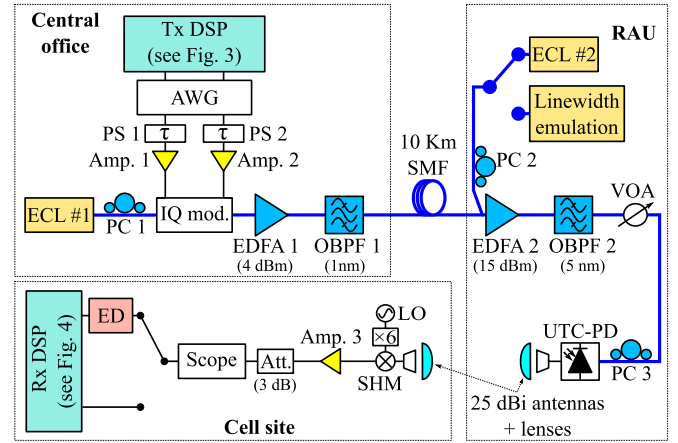


Fig. 5. Experimental arrangement used in the transmission experiments. The SSB signals were recovered using the Rx path with the digital envelope detector. For BB signals, the received waveform was directly fed into the DSP routine shown in Fig. 4. ECL: external cavity laser, AWG: arbitrary waveform generator, VOA: variable optical attenuator, UTC-PD: uni-travelling carrier photodiode, EDFA: erbium doped fibre amplifier, PC: polarization controller, SMF: single mode fibre, SHM: second-harmonic mixer.

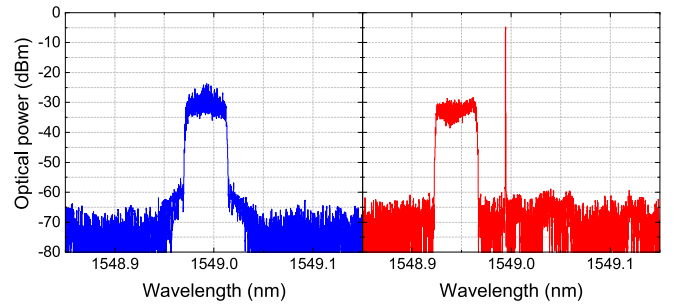


Fig. 6. Optical spectra of (a) BB signal, and (b) SSB signal after transmission through 10 km of single mode fibre.

C. Experimental Arrangement

The complete experimental arrangement used in the transmission experiments is shown in Fig. 5. On the transmitter side, an external cavity laser (ECL #1) with a linewidth of 11 kHz and a wavelength of 1549 nm was used for data modulation. For BB modulation, the biases for the I- and Q-components of the IQ modulator were set at the null point. On the other hand, for SSB modulation, the biasing points were adjusted to increase or decrease the CFSR depending on f_{SC} as described in Section II. At low f_{SC} , the biasing points were tuned towards the quadrature point to increase the CFSR. Conversely, at high f_{SC} , the modulator biases were set closer to the minimum transmission point to decrease the CFSR. After optical modulation, the signal was transmitted through 10 km of optical single mode fibre (SMF). The generated optical signals for both (a) BB and (b) SSB modulations are shown in Fig. 6 after fibre transmission (i.e., at the entrance of the RAU). As can be seen from Fig. 5, two phase shifters were inserted after the AWG. This was done to make sure no time delay existed between the I- and Q-channels and allowed us to achieve an OSSR of about 30 dB (Fig. 6(b)), which matches well with the measured ER of our IQ-modulator (30.5 dB).

TABLE I
COMPONENTS USED IN THE TRANSMISSION EXPERIMENTS

Component	Manufacturer; version	Parameters
Amp. 1, Amp. 2	SHF; S807 B	Gain: 23 dB NF: not available
Amp. 3	Microsemi; AML618P3502	Gain: 35 dB NF: 4 dB
ECL#1, ECL#2	Pure Photonics; PPCL100	$\Delta\nu$: 11 kHz (measured) Power: 15 dBm
IQ mod.	Covega; 086-40-16-SFF	ER: 30.5 dB (measured) Bandwidth: 18 GHz
SHM	VDI; WR3.4SHM	Conv. loss: 14 dB NF: \sim 30 dB
LO	R&S; SMF100A	SSB phase noise: -120 dBc (@10 GHz, 10 kHz offset)

NF: noise figure, $\Delta\nu$: linewidth

When no linewidth emulation was carried out, the incoming optical signal was combined with a second ECL (ECL #2) with a 11 kHz linewidth and a wavelength of 1551 nm (the frequency difference between the two lasers was 250 GHz). After optical amplification and filtering, the signal and the unmodulated tone were sent to a uni-travelling carrier photodiode (UTC-PD). Horn antennas with a gain of 25 dBi were used for both transmission and reception and placed at a distance of 0.3 m from each other. A pair of lenses were inserted between the two antennas to increase the collimation of the THz beam and achieve a higher transmission gain. In the receiver, after down-conversion in the SHM, the signal was digitized by a real-time scope working at a sampling rate of 80 Gsample/s. After this, the CSPP was calculated from the recorded waveform and then the digital ED, consisting in a brick-wall band pass filter, a square-law operation, and a brick-wall low pass filter, was applied to recover the SSB signals. In the case of BB transmission, the digitized signal was directly fed into the DSP routine shown in Fig. 4. In Table I, the main features of the components used in the transmissions are summarized.

D. Linewidth Emulation

For linewidth tuning, ECL #2 was modulated by several white frequency noise sequences using a second IQ modulator [19]. The linewidth of the THz signal was estimated by measuring the frequency modulation (FM) noise spectrum of the heterodyne signal between ECL #1 and the output of the linewidth emulator at a frequency of around 6.5 GHz. The beat note at this frequency was recorded by a 20 Gsample/s oscilloscope and processed digitally offline (down-converted, filtered and resampled) before computing the white frequency noise component. The measured Lorentzian linewidths of the heterodyne signal (i.e., including ECL #1 linewidth) for the three different emulated linewidths used in this experiment were 229 kHz, 493 kHz and 905 kHz (for emulated linewidths of 200 kHz, 500 kHz, and 1 MHz, respectively).

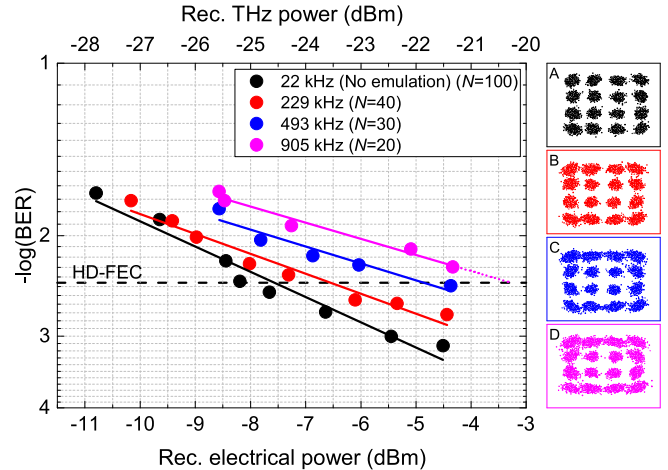


Fig. 7. BER versus received electrical power for BB signals and different combined optical linewidths. Insets A, B, C, and D: constellation diagrams at the lowest BER values for 22 kHz, 229 kHz, 493 kHz, and 905 kHz linewidths, respectively. N denotes the size of the averaging filter in the VV algorithm.

IV. RESULTS

In this section, we show the effect of RAU laser linewidth on the link BER performance when employing: (a) BB signals and (b) SSB signals. The BER is plotted versus the received electrical power (measured from the waveforms recorded by the real-time scope) and THz power (after the Rx antenna), which is calculated from the parameters in Table I, assuming 1-dB waveguide losses and taking into account the 3-dB attenuator before the real-time scope. For all BER curves, the maximum input power to the UTC-PD (measured with an in-line power meter inserted before the fibre feeding the PD) was limited to 12 dBm to avoid saturation effects. The analysis and comparison of the results presented in this section is performed in Section IV.

A. BB Signals

The BER obtained for the BB signals and the four different combined optical linewidths is shown in Fig. 7. For each linewidth, the block length of the VV algorithm (N), was optimized for the highest received power and then kept constant over the BER measurements. The intersection of each curve with the hard decision (HD)-FEC limit (BER of $3.8 \cdot 10^{-3}$) will be used in the next section to compare the relative performance of SSB and BB signals (for the 905 kHz linewidth, where the HD-FEC limit could not be reached, the linear fit was extrapolated (dotted pink line) to get the intersection point).

B. SSB Signals

For a given roll-off factor, the choice of f_{SC} determines the width of the GB between signal and carrier and, hence, the spectral efficiency of the SSB signal. To achieve a spectral efficiency similar to that of BB signals, f_{SC} should be as low as possible. To determine the maximum spectral efficiency achievable with our system, we increased f_{SC} in steps of 1.25 GHz ($0.25 \times$ symbol rate) until a BER below the HD-FEC limit

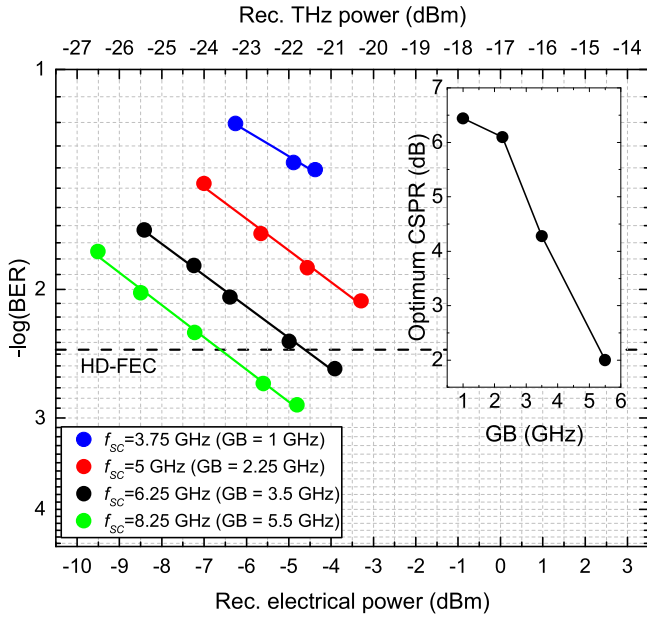


Fig. 8. BER versus received electrical power for SSB signals with different GBs. The inset shows the optimum CSPR versus the GB.

was obtained. In Fig. 8, the BER versus the received power is shown for different f_{SC} values. As can be seen, a subcarrier frequency of 6.25 GHz (GB of 3.5 GHz) was enough to satisfy the HD-FEC requirement. This f_{SC} value was, therefore, the one used in the linewidth emulation measurements. The BER curve for a GB as wide as the BW (GB of 5.5 GHz) is also included to show the performance of the system with no SSBI. In all the cases, the CSPR was optimized for the highest value of received power and then kept constant over each BER curve measurement. The optimum value obtained for each GB is plotted in the inset of Fig. 8. As expected (see Section II), the optimum CSPR decreases as the GB is increased. The results of the linewidth emulation for a f_{SC} of 6.25 GHz and the same combined linewidths of Fig. 7 (the linear fits for the 22 kHz and 905 kHz BB curves are included for reference) are plotted in Fig. 9.

Given the large transmission windows found at THz frequencies (up to 70 GHz in the window centred at 287 GHz [26]), the use of large GBs to combat the SSBI may be acceptable in THz SSB signals. However, if the spectral efficiency is a critical parameter of the intended THz-over-fibre link (because of congestion in the optical part of the link, for instance), employing DSP for SSBI mitigation can be useful. From all the algorithms that have been proposed for this purpose, the Kramers-Kronig (KK) receiver (first demonstrated in [15]) has shown promising results in DD optical networks [27]. As long as the SSB signal has a sufficiently high CSPR, this scheme can reconstruct the optical phase of the data-carrying signal reaching the envelope detector. For practical purposes, this means eliminating the DD terms and, thus, the SSBI.

To see the spectral efficiency gain that can be achieved with this algorithm, the KK receiver was implemented after envelope detection and before the coherent Rx DSP (see Fig. 5). The KK

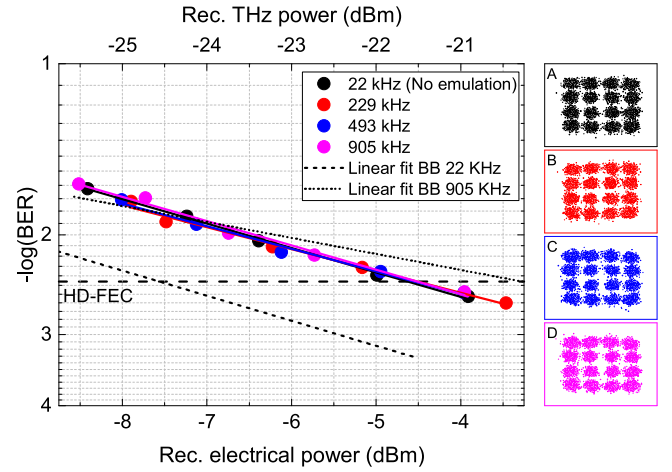


Fig. 9. BER versus received electrical power for SSB signals with f_{SC} of 6.25 GHz and different combined optical linewidths. Insets A, B, C, and D: constellation diagrams at the lowest BER value for the 22 kHz, 229 kHz, 493 kHz and 905 kHz linewidths respectively.

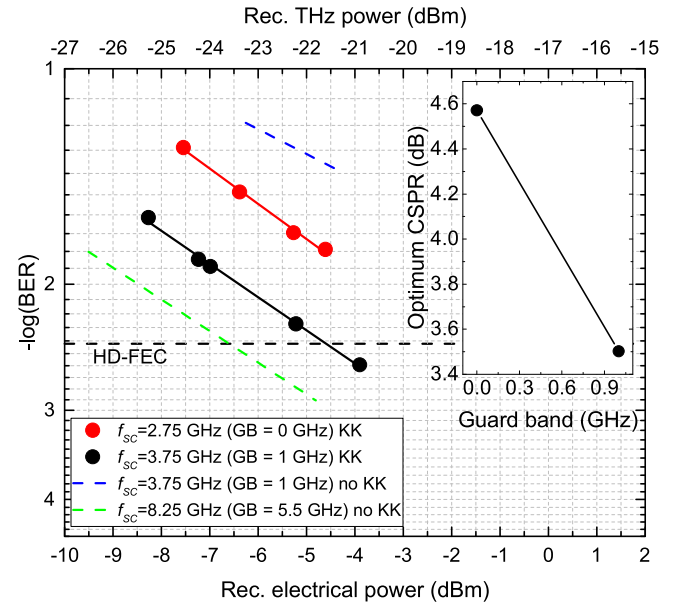


Fig. 10. BER versus received electrical power for SSB signals using the KK receiver. The inset shows the optimum CSPR versus the GB for the two curves taken with the KK receiver.

algorithm can be written as follows:

$$A_{KK}(t) = \text{sqr}t(S_{ED}(t)), \quad (7)$$

$$\varphi_{KK}(t) = \mathbf{H}[\ln(A_{KK}(t))], \quad (8)$$

$$S_{KK}(t) = A_{KK}(t) \cdot \exp(j\varphi_{KK}(t)), \quad (9)$$

where S_{ED} is the signal after envelope detection, and A_{KK} and φ_{KK} are the amplitude and phase terms of the KK signal, which is here denoted as S_{KK} . In Fig. 10, the BER curves obtained with the KK algorithm are plotted for different values of f_{SC} . As can be seen, although the implementation of this algorithm was not sufficient to successfully recover a signal with no GB (at a maximum optical input power to the UTC of around 12 dBm), it did allow the recovery of a signal with a GB as low as 1 GHz. For comparison, the linear-fit curves for

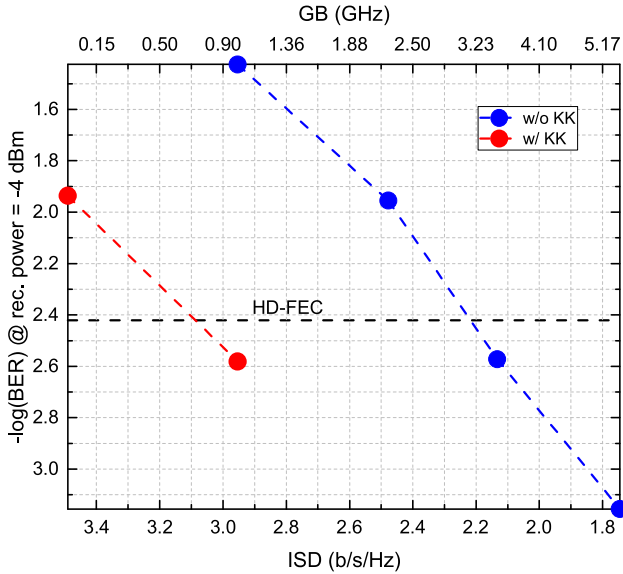


Fig. 11. BER at a received electrical power of -4 dBm versus the net ISD of the transmitted SSB signal.

GBs of 1 GHz and 5.5 GHz without the KK receiver are also shown in Fig 9. It is worth noting that, in the KK algorithm, a high oversampling rate is required to account for the square-root and logarithm operations [28]. In our case, sample rates of 6 sample/symbol and 9 sample/symbol were used for f_{SC} of 2.75 GHz and 3.75 GHz, respectively. In a practical system using a THz ED, an AC coupled electrical amplifier may be used after the ED to add electrostatic discharge protection. If that is the case, the DC component of the received signal will be blocked. Since this term is necessary to correctly perform the KK receiver, one may emulate it digitally by adding a real number to the digitized signal [29].

V. DISCUSSION

A. Spectral Efficiency of SSB Signals

In Fig. 11, the BER at a received power of -4 dBm (which is close to the maximum power recorded by the scope in the transmission experiments) is plotted as a function of the net information spectral density (ISD) of the SSB signals (both w/o and w/ the KK receiver). The net ISD, which is just another way to refer to the spectral efficiency of a signal, is defined as: $r \times (R_s \cdot \log_2(M)/BW)$, where r is the code rate of the FEC process (here assumed to be 0.96), R_s is the symbol rate, M is the modulation order, and BW is the bandwidth taken by the signal (which in case of single-subcarrier SSB signals is equal to $GB + R_s(1 + \alpha)$, where α is the Nyquist roll-off factor). It should be noted that, in the cases where the maximum received power was less than -4 dBm, the linear fit was extrapolated to find the intersection point. As expected, in both cases, the BER performance improves when the GB is increased (i.e., the ISD is reduced).

The maximum ISD achievable with a SSB signal is obtained when no GB is used and is equal to that of the sideband signal. In our case, the sideband was a 16-QAM signal with a roll-off factor of 0.1, so the maximum achievable net ISD was 3.49 b/s/Hz (this

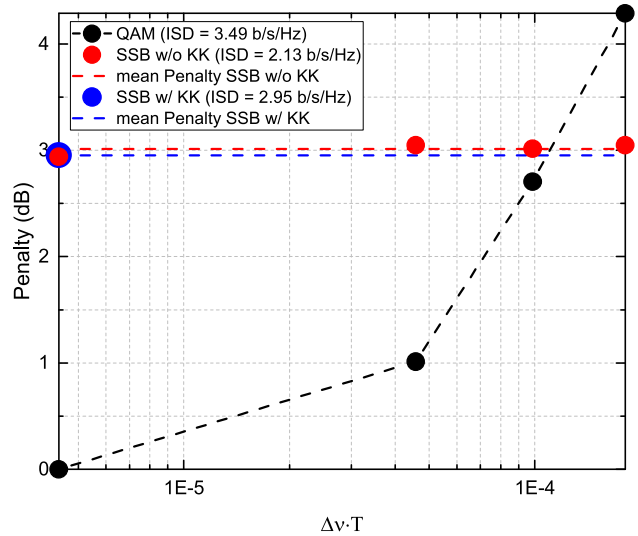


Fig. 12. Penalty at a BER of $3.8 \cdot 10^{-3}$ due to combined linewidth. Points represent the intersection of the linear fits with the HD-FEC threshold. In the case of the SSB w/o KK scheme, the penalty is assumed to remain constant with linewidth (this is experimentally verified for SSB signals w/o the KK receiver).

value of ISD corresponds to the left vertical axis in Fig. 11). Compared to this upper limit, and when the KK receiver was not used, the ISD of the SSB signal had to be reduced by 39% (ISD of 2.13 b/s/Hz) to satisfy the HD-FEC requirement. On the other hand, using the KK receiver, a BER below the FEC limit could be achieved with a SSB signal with an ISD as high as 2.95 b/s/Hz, which represents just a 15% reduction with respect to the upper limit (or an improvement of 38% with respect to the SSB signal w/o KK).

B. Linewidth Tolerance

In Fig. 12, the penalty at the HD-FEC threshold versus the (combined linewidth) \times (symbol period) product (which is the figure of merit of carrier recovery algorithms) is plotted for both the BB and the SSB signals. As can be seen, in the case of BB signals, there is a clear penalty associated with wider linewidths. As mentioned in Section I, this penalty comes from the shortening of the averaging filter to track the faster symbol deviations introduced by broader linewidths. On the other hand, for the SSB signals, the penalty difference at the HD-FEC limit is very small (less than 0.1 dB). These penalty differences are likely to be due to causes other than laser linewidth, such as drifts in the biasing points of the IQ modulators (which, in the case of the data modulator, can cause the CSPR to deviate from the optimum one, or, in the case of the linewidth-emulation modulator, to introduce relative intensity noise), for instance. It can be concluded, therefore, that the sensitivity of the SSB system is not affected by white frequency noise.

Using the dashed lines for each type of signal (for the case w/ the KK receiver we assume the penalty remains constant and extrapolate the value obtained when no linewidth emulation is performed), one can see that the penalty of BB signals becomes higher than that of the SSB signals, both w/o and w/ KK receiver, for a $(\Delta\nu \cdot T)$ product of approximately $1.1 \cdot 10^{-4}$. Assuming a linewidth for the RAU laser of 2 MHz (which is similar to the

ones reported for foundry-fabricated DFB lasers [30]) and of 100 kHz for the laser in the CO (linewidth of off-the-shelf ECL lasers), a combined linewidth of 2.1 MHz is obtained, which, solving for T^{-1} , yields a symbol rate of approximately 19 GBd. For symbol rates lower than this, the envelope detection of SSB signals should be more effective.

On the other hand, if we assume fixed symbol rates of 10 GBd and 5 GBd, combined linewidths of 1.1 MHz and 0.55 MHz, respectively, are obtained. Assuming a CO laser linewidth of 100 kHz, this translates into RAU-laser linewidths of 1 MHz and 0.45 MHz, respectively. For RAU-laser linewidths wider than this, the SSB approach should be more effective. These results seem to indicate, hence, that the envelope detection of SSB signals can offer good prospects for the deployment of low-cost RAU units for THz-over-fibre systems without necessarily compromising the spectral efficiency of such links.

VI. CONCLUSION

We have characterized the sensitivity of a THz-over-fibre system based on SSB signals & envelope detection to optical LO linewidth. Before doing so, we have investigated the impact of GB in order to determine the highest spectral efficiency allowed by our system. Finally, we have compared the results with those obtained when using BB signals & carrier recovery at the receiver. Using 5 GBd 16-QAM signals, we experimentally confirm that the SSB scheme, unlike the BB approach, shows no penalty associated with linewidth. Furthermore, we find that, for a total optical linewidth wider than 0.55 MHz, this approach yields better sensitivity. This, however, is achieved at the expense of reducing the ISD of the SSB signal by 39% compared to the maximum achievable (which is obtained when no GB is used between carrier and sideband). On the other hand, using the KK receiver to mitigate the SSBI, only a 15% reduction of the ISD was needed to meet the HD-FEC requirement. We believe, therefore, that the envelope detection of SSB signals is a promising solution to enable the use of low-cost free-running lasers in THz-over-fibre systems.

ACKNOWLEDGMENT

The authors would like to thank Frédéric van Dijk of Alcatel Thales III-V Lab for providing the UTC-PD.

REFERENCES

- [1] H. Shams, M. J. Fice, L. Gonzalez-Guerrero, C. C. Renaud, F. Van Dijk, and A. J. Seeds, "Sub-THz wireless over fiber for frequency band 220–280 GHz," *J. Lightw. Technol.*, vol. 34, no. 20, pp. 4786–4793, Oct. 2016.
- [2] T. Nagatsuma *et al.*, "Terahertz wireless communications based on photonics technologies," *Opt. Express*, vol. 21, no. 20, 2013, Art. no. 23736.
- [3] A. J. Seeds, H. Shams, M. J. Fice, and C. C. Renaud, "TeraHertz photonics for wireless communications," *J. Lightw. Technol.*, vol. 33, no. 3, pp. 579–587, Feb. 2015.
- [4] H. Shams *et al.*, "100 Gb/s multicarrier THz wireless transmission system with high frequency stability based on a gain-switched laser comb source," *IEEE Photon. J.*, vol. 7, no. 3, Jun. 2015, Art. no. 7902011.
- [5] T. Shao *et al.*, "Phase noise investigation of multicarrier Sub-THz wireless transmission system based on an injection-locked gain-switched laser," *IEEE Trans. THz Sci. Technol.*, vol. 5, no. 4, pp. 590–597, Jul. 2015.
- [6] S. Mandelli *et al.*, "Phase noise impact on directly detected optical OFDM transmission in uncompensated links," in *Proc. Int. Conf. Transparent Opt. Netw.*, 2016, pp. 5–8.
- [7] K. Balakier *et al.*, "Demonstration of photonic integrated Rau for millimetre-wave gigabit wireless transmission," in *Proc. IEEE Topical Meet. Microw. Photon.*, 2016, vol. 6, pp. 344–347.
- [8] M. S. Erklilnc *et al.*, "Bidirectional wavelength-division multiplexing transmission over installed fibre using a simplified optical coherent access transceiver," *Nature Commun.*, vol. 8, no. 1, pp. 1–10, 2017.
- [9] M. Seimetz, "Laser linewidth limitations for optical systems with high-order modulation employing feed forward digital carrier phase estimation," in *Proc. Conf. Opt. Fiber Commun. Fiber Opt. Eng. Conf.*, 2008, pp. 2–4.
- [10] M. Selmi, Y. Jaouen, and P. Ciblat, "Accurate digital frequency offset estimator for coherent PoIMux QAM transmission systems," in *Proc. 35th Eur. Conf. Opt. Commun.*, 2009, no. 1, pp. 3–4.
- [11] I. Fatadin, D. Ives, and S. J. Savory, "Carrier phase recovery for 16-QAM using QPSK partitioning and sliding window averaging," *IEEE Photon. Technol. Lett.*, vol. 26, no. 9, pp. 854–857, May 2014.
- [12] T. Pfau, S. Hoffmann, and R. Noé, "Hardware-efficient coherent digital receiver concept with feedforward carrier recovery for M-QAM constellations," *J. Lightw. Technol.*, vol. 27, no. 8, pp. 989–999, Apr. 2009.
- [13] X. Zhou, "Efficient clock and carrier recovery algorithms for single-carrier coherent optical systems: A systematic review on challenges and recent progress," *IEEE Signal Process. Mag.*, vol. 31, no. 2, pp. 35–45, Mar. 2014.
- [14] K. Kikuchi, "Fundamentals of coherent optical fiber communications," *J. Lightw. Technol.*, vol. 34, no. 1, pp. 157–179, Jan. 2016.
- [15] H. Voelcker, "Demodulation of single-sideband signals via envelope detection," *IEEE Trans. Commun. Technol.*, vol. 14, no. 1, pp. 22–30, Feb. 1966.
- [16] R. Hui, B. Zhu, R. Huang, C. Allen, K. Demarest, and D. Richards, "10-Gb/s SCM fiber system using optical SSB modulation," *IEEE Photon. Technol. Lett.*, vol. 13, no. 8, pp. 896–898, Aug. 2001.
- [17] M. F. Hermelo, P.-T. (Boris) Shih, M. Steeg, A. Ng'oma, and A. Stöhr, "Spectral efficient 64-QAM-OFDM terahertz communication link," *Opt. Express*, vol. 25, no. 16, 2017, Art. no. 19360.
- [18] I. Aldaya, G. Campuzano, C. Gosset, and G. Castanon, "Phase-insensitive RF envelope detection allows optical heterodyning of MHz-linewidth signals," *IEEE Photon. Technol. Lett.*, vol. 25, no. 22, pp. 2193–2196, Nov. 2013.
- [19] Z. Zan and A. J. Lowery, "Experimental demonstration of a flexible and stable semiconductor laser linewidth emulator," *Opt. Express*, vol. 18, no. 13, pp. 13880–13885, 2010.
- [20] S. Jia *et al.*, "THz photonic wireless links with 16-QAM modulation in the 375–450 GHz band," *Opt. Express*, vol. 24, no. 21 2016, Art. no. 23777.
- [21] Y. Zhu, M. Jiang, X. Ruan, C. Li, and F. Zhang, "112Gb/s single-sideband PAM4 WDM transmission over 80km SSMF with Kramers-Kronig receiver," in *Proc. Opt. Fiber Commun. Conf. Expo.*, 2018, paper Tu2D.2.
- [22] J. Ma and W. Zhou, "Joint influence of the optical carrier-to-sideband ratio and guard band on direct-detection SSB-OOFDM system," *IEEE Photon. J.*, vol. 7, no. 5, Oct. 2015, Art. no. 7801713.
- [23] M. S. Erkilinc *et al.*, "Spectrally efficient WDM nyquist pulse-shaped subcarrier modulation using a dual-drive Mach-Zehnder modulator and direct detection," *J. Lightw. Technol.*, vol. 34, no. 4, pp. 1158–1165, Feb. 2016.
- [24] F. C. Abrecht *et al.*, "Pre-equalization technique enabling 70 Gbit/s photonic-wireless link at 60 GHz," *Opt. Express*, vol. 24, no. 26, 2016, Art. no. 30350.
- [25] M. G. Taylor, "Phase estimation methods for optical coherent detection using digital signal processing," *J. Lightw. Technol.*, vol. 27, no. 7, pp. 901–914, Apr. 2009.
- [26] IEEE 802.15, "TG3d technical requirements document," 2016. [Online]. Available: http://www.ieee802.org/15/pub/index_TG3d.html
- [27] Z. Li *et al.*, "SSBI mitigation and the kramers-kronig scheme in single-sideband direct-detection transmission with receiver-based electronic dispersion compensation," *J. Lightw. Technol.*, vol. 35, no. 10, pp. 1887–1893, May 2017.
- [28] M. S. A. Mecozzi and C. Antonelli, "Kramers-Kronig coherent receiver," *Optica*, vol. 3, no. 11, pp. 1220–1227, 2016.
- [29] Y. Zhu, K. Zou, X. Ruan, and F. Zhang, "Single carrier 400 G transmission with single-ended heterodyne detection," *IEEE Photon. Technol. Lett.*, vol. 29, no. 21, pp. 1788–1791, Nov. 2017.
- [30] K. Balakier *et al.*, "Optical injection locking of monolithically integrated photonic source for generation of high purity signals above 100 GHz," *Opt. Express*, vol. 22, no. 24, 2014, Art. no. 29404.